American Mineralogist, Volume 89, pages 1655–1666, 2004

Origin of diffuse superstructure reflections in labuntsovite-group minerals

THOMAS ARMBRUSTER,[1,*] SERGEY V. KRIVOVICHEV,[2] THOMAS WEBER,[3] EDWIN GNOS,[4] NATALIA N. ORGANOVA,[5] VIKTOR N. YAKOVENCHUK,[6] AND ZOYA V. SHLYUKOVA[5]

[1]Laboratorium für chemische und mineralogische Kristallographie, Universtät Bern, Freiestrasse 3, CH-3012 Bern, Switzerland
[2]Department of Crystallography, St. Petersburg State University, University Emb. 7/9, 199034 St. Petersburg, Russia
[3]Laboratory of Crystallography, ETH, ETH-Zentrum, CH-8092 Zurich, Switzerland
[4]Institut für Geologie, Universtät Bern, Baltzerstr. 1, CH-3012 Bern, Switzerland
[5]Institute of Geology of Ore Deposits, Petrology, Mineralogy and Geochemistry, Russian Academy of Sciences, Staromonetny per. 35, 109017 Moscow, Russia
[6]Geological Institute, Kola Science Center of the Russian Academy of Sciences, 184200 Apatity, Russia

ABSTRACT

The average crystal structures of two natural porous titanosilicates of the labuntsovite group, lemmleinite-Ba and lemmleinite-K, ideally $Na_4K_4Ba_2Ti_8(Si_4O_{12})_4O_4(OH)_4\cdot 8H_2O$ and $Na_4K_4K_2Ti_8(Si_4O_{12})_4O_2(OH)_6\cdot 8H_2O$, respectively, have been refined from single crystal X-ray diffraction data. Both samples represent an extensive solid solution with labuntsovite sensu strictu $Na_4K_4D_2Ti_8(Si_4O_{12})_4O_4(OH)_4\cdot 10H_2O$ where D = Mn, Fe, and Mg. In addition to the sharp Bragg reflections both crystals, space group *C*2/*m*, *a* = 14.3, *b* =13.8, *c* = 7.75 Å, β = 117°, exhibit diffuse layers at *c**/2 intervals indicating faulty superstructures with *c* = 15.7 Å. The diffuse layers consist of two types of reflections. The dominant type is strongly diffuse and smeared along **a*** indicating an *I*-centered Bravais lattice. The other type is very sharp but also weak and is in agreement with a *C*-centered lattice. Models for both superstructures have been developed on the basis of crystal-chemical principles and their theoretical diffraction patterns have been calculated and compared with the observed diffuse layers yielding excellent qualitative agreement.

X-ray structure refinements of the average structure at –160 and 22 °C indicate temperature independent (static) disorder of Ti within rather rigid TiO_6 octahedra connected to chains that extend along **a.** This Ti disorder is interpreted in terms of long-range order of OH and O in the superstructures where these anions occupy the corner-connecting octahedral apices in an ordered fashion. An additional effect of OH, O order is an ordered arrangement of extraframework Ba (K) that only bonds to O but not to OH sites exposed on the channel walls.

Temperature dependent cell dimensions between –160 and +200 °C suggest a phase transition at ca. –80 °C. However, the structural data obtained from the average structures, refined at –160 and 22 °C, did not allow us to draw crystal-chemical conclusions about the nature of the phase transition. Dehydration of the investigated lemmleinite-Ba starts at ca. 150 °C leading to increasing extraframework disorder and decreasing crystal quality as evidenced by strong smearing of the originally sharp Bragg reflections.

INTRODUCTION

Labuntsovite-group minerals (Chukanov et al. 2002) comprise porous titanium and niobium silicates with a common tetrahedral-octahedral framework topology formed by chains of corner-sharing octahedra (Ti, Nb) extending along **a**, which are cross-linked by four-membered rings of tetrahedra (Si). Depending on the configuration of the octahedral chains two subgroups are distinguished: (1) The orthorhombic members, space group *Pbam*, *a* = 7.4 *b* = 14.2, *c* =7.1 Å (nenadkevichite, M = Nb and korobitsynite, M = Ti) and (2) a variety of monoclinic minerals, space group *C*2/*m*, *a* = 14.3, *b* =13.8, *c* =7.75 or 15.7 Å, β = 117°. In addition to the substitution of Ti by Nb, the monoclinic labuntsovite-group minerals are distinguished by different substitutions in the porous voids. In the context of this study, the labuntsovite and lemmleinite monoclinic subgroups (Chukanov et al. 2002) are of importance.

In labuntsovite, chains of Ti octahedra are in addition to the four-membered rings of tetrahedra cross-linked by an edge-sharing octahedron (D = Mn, Fe, Mg) where the additional two octahedral apices are formed by H_2O molecules. The remaining porous space is filled by Na, K, and H_2O. The idealized formula of labuntsovite may be written as $Na_4K_4D_2Ti_8(Si_4O_{12})_4O_4(OH)_4\cdot 10H_2O$. A hyphenated suffix characterizes the species with different octahedral D ions (e.g., labuntsovite-Mn etc.).

Members of the lemmleinite subgroup have no edge-connected D octahedra but instead K or Ba (C site) occupies the same position as the H_2O molecule forming the two octahedral D-site apices in labuntsovite. Thus the substitution may be written as

$$(Fe,Mg,Mn,Zn)^D + 2H_2O^C \rightarrow \square^D + 2(K, 0.5\ Ba)^C \quad (1)$$

The idealized formula of lemmleinite-Ba is $Na_4K_4Ba_2Ti_8(Si_4O_{12})_4O_4(OH)_4\cdot 8H_2O$, whereas that of lemmleinite-K is $Na_4K_4K_2$

* E-mail: thomas.armbruster@krist.unibe.ch

$Ti_8(Si_4O_{12})_4O_2(OH)_6 \cdot 8H_2O$.

After Semenov and Burova (1955) described and defined labuntsovite from the albitic pegmatites of the Kola peninsula, Milton et al. (1958) discovered authigenic labuntsovite in unmetamorphosed sediments of the Green River formation, Wyoming. Their labuntsovite had the composition $Na_{4.39}K_{3.65}Ba_{1.4}Mg_{1.14}(Fe^{3+}_{0.13}Nb_{0.05}Ti_{7.68})(Si_{3.95}Al_{0.05}O_{12})_4(O,OH)_8 \cdot 12H_2O$ (sum of cation charges: 108.06) and should thus be considered a solid-solution member between lemmleinite-Ba and labuntsovite-Mg. Because Milton et al. (1958) determined a doubled *c* axis of 2 × 7.75 = 15.5 Å and space group *I*2/*m*, this mineral was later named paralabuntsovite (Chukanov et al. 2002).

The crystal structure of labuntsovite was solved by Golovastikov (1973) with crystals from the Kola peninsula (Semenov and Burova 1955). Unfortunately, no exact chemical composition was given but Golovastikov (1973) assigned the studied crystal to the "brown" variety of labuntsovite for which he cites the approximate composition $K_{3.76}Na_{2.54}Ca_{0.79}Ba_{1.39}Mn_{0.79}Fe_{0.44}Mg_{0.26}(Ti_{7.78}Nb_{0.26})(Si_4O_{12})_4(O,OH)_8 \cdot nH_2O$ (sum of cation charges: 110.06). Note that this composition is close to a 1:1 solid-solution member of the labuntsovite-lemmleinite series. In the course of the structure refinement in space group *C*2/*m* with a *c* dimension of ca. 7.75 Å (note that Golovastikov used a non-standard setting in his original paper which is here transformed to the standard setting), Golovastikov (1973) was perplexed by the short distance of ca. 2.1 Å between the D octahedron and (K, Ba) at the C site. To solve this ambiguity he doubled the *c* axis and transformed his structure with *c* = 7.75 Å and space group *C*2/*m* to the Milton et al. (1958) cell with *c* = 15.5 Å and space group *I*2/*m* by developing an ordering pattern along **b** of framework cavities alternately occupied by D (Mn,Fe,Mg) and C (K,Ba) sites. Diffraction evidence for the modeled "superstructure" were weak, "diffuse strokes" at halved *c** recorded on long-exposure oscillation X-ray photographs. Golovastikov (1973) concluded his structural study with the statement: "Refinement of these "errors" in the structure awaits further research." Along this line, Organova et al. (1976, 1980, 1981) investigated several "labuntsovites," including material from the Green River formation, originally studied by Milton et al. (1958). In their very interesting but almost unknown paper, Organova et al. (1980) considered the problem of order and disorder in minerals of the labuntsovite group. According to these authors, there are three characteristic types of diffraction patterns observed for labuntsovite-group minerals: (1) patterns that have sharp "superstructure" reflections corresponding to space group *I*2/*m* and a "doubled" *c* dimension of ca. 15.5 Å; (2) patterns that have only sharp reflections that can be indexed with a unit cell of *c* ~ 7.75 Å in space group *C*2/*m*; (3) patterns that have sharp reflections indexable in a unit cell with *c* ~ 7.75 Å but with additional diffuse reflections, streaked along **a***, that can be indexed with the *I*2/*m* unit cell. Type 1 and 2 patterns were considered to result from completely ordered and disordered arrangements, respectively, whereas type 3 patterns were interpreted to result from arrangements with an intermediate degree of order. Organova et al. (1976) pointed out that the structural nature of order-disorder in labuntsovite-group minerals is based on the arrangement of C and D sites expressed by Equation 1 above. This is in agreement with the suggestion of Golovastikov (1973) and our results discussed below. Organova et al. (1980) noted that the presence of the diffuse reflections, streaked along **a***, indicates that thin layered domains, parallel to (100), of the ordered labuntsovite structure are shifted relative to each other by ±*c*/2. The thinner these layered domains, the more diffuse are the respective reflections. In the completely disordered labuntsovites, these reflections are absent and the diffraction pattern can be indexed with a *C*-centered cell with *c* ~ 7.75 Å. Organova et al. (1980) attempted to correlate the degree of ordering in labuntsovites with thermodynamic conditions of their formation. Although the low-temperature origin of the labuntsovite studied by Milton et al. (1958) (*T* ~ 200 °C) is in agreement with its *I*2/*m* unit cell and "doubled" *c* axis (ordered arrangement), there was no such evident correlation for the other labuntsovite-group minerals studied by Organova et al. (1980, 1981).

Thirty years after its discovery by Golovastikov (1973) the present paper aims for a qualitative interpretation of diffuse scattering in the labuntsovite-group minerals by using a state-of-the-art area detector to monitor diffraction data.

Sample characterization

Both samples originate from the Khibiny alkaline complex, Kola peninsula, Russia. Sample A is from the collection of co-author V.N.Y. and was previously briefly described by Yakovenchuk et al. (1999). It comprises pale yellow prolate crystals up to 0.7 mm in maximum dimension. Sample B is from the batch of crystals studied by Organova et al. (1976, 1981). It represents orange prismatic crystals irregularly intergrown to aggregates. The minerals were analyzed with a Cameca SX-50 microprobe using beam conditions of 15 kV and 10 nA, wavelength-dispersive spectrometers, and an enlarged spot size of ca. 15 µm. Natural and synthetic minerals were used as standards: orthoclase Si*K*α (TAP) and K*K*α (PET), anorthite Al*K*α (TAP) and Ca*K*α (PET), almandine Fe*K*α (LiF), tephroite Mn*K*α (LiF), spinel Mg*K*α (TAP), celestine Sr*L*α (PET), barite Ba*L*α (LiF), ilmenite Ti*K*α (LiF), albite Na*K*α (TAP), $KTaO_3$ Ta*L*α (LiF), $KNbO_3$ Nb*L*α (PET), and zircon Zr*L*α (TAP). Data for Ba, Sr, Ti, Zr, Ta, and Nb were collected for 30 seconds, all other elements for 20 seconds. Pb, Zn, Cr, and Cu concentrations were found below detection limit in qualitative wavelength-dispersive scans, and hence were not analyzed further. Results are given in Table 1.

On the basis of the chemical composition (Chukanov et al. 2002), samples A and B are considered to be lemmleinite-Ba and lemmleinite-K, respectively.

X-ray diffraction experiments

Initially both crystals (A1 and B1) were studied with a Bruker platform 1K CCD area detector (graphite monochromated Mo*K*α X-radiation) at 22 and –150 °C (liquid nitrogen cooling system). Both crystal exhibited at both temperatures sharp X-ray reflections, which could be indexed with a conventional *C*-centered labuntsovite cell of ca. *a* = 14.3, *b* = 13.8, *c* = 7.75 Å, β = 117°, in addition to diffuse features occurring at c*/2 intervals, suggesting doubling of the *c* axis dimension.

Because more precise and accurate cell dimensions can be measured with a point detector mounted on a four-circle machine (Herbstein 2000), crystals A1 and B1 were subsequently transferred to an Enraf Nonius CAD4-diffractometer (graphite monochromated Mo*K*α X-radiation) to collect reference structural data at room temperature.

In addition, temperature dependent cell dimensions based on the angular setting of 22 reflections with θ >20° were collected for crystal A1 between –160° and +200 °C. Low temperature was achieved with a conventional liquid nitrogen blower whereas high temperature was obtained by means of a self-constructed

TABLE 1. Electron microprobe analyses of two labuntsovite-group minerals

	Mean n = 15	Min. n =15	Max. n =15	esd	Mean n = 29	Min. n = 29	Max. n = 29	esd
Sample	A	A	A	A	B	B	B	B
SiO2	38.17	36.95	39.04	0.47	39.05	38.66	39.37	0.24
TiO2	23.59	22.92	24.06	0.34	22.56	21.75	23.11	0.34
Al2O3	0.05	0.03	0.07	0.01	0.00	0.00	0.03	0.01
FeO	0.74	0.58	0.84	0.07	2.03	1.90	2.24	0.09
MnO	1.85	1.60	2.03	0.10	0.04	0.00	0.07	0.03
MgO	0.25	0.14	0.31	0.05	0.38	0.32	0.45	0.04
CaO	0.01	0.00	0.02	0.01	0.00	0.00	0.02	0.01
SrO	0.00	0.00	0.00	0.00	0.00	0.00	0.00	0.00
BaO	10.75	9.76	11.83	0.64	5.85	4.54	7.75	1.05
Na2O	5.38	4.96	5.68	0.19	5.05	4.87	5.23	0.11
K2O	6.91	6.72	7.02	0.08	9.82	9.20	10.35	0.39
ZrO2	0.12	0.06	0.19	0.04	0.00	0.00	0.02	0.01
Nb2O5	1.08	0.53	2.20	0.49	4.06	2.74	4.94	0.56
Ta2O5	0.01	0.00	0.09	0.03	0.03	0.00	0.14	0.05
Total	88.92	88.32	89.98	0.43	88.89	88.11	89.46	0.38
Sample	A				B			
Si	15.975				16.000			
Ti	7.425				6.951			
Al	0.025				0			
Fe	0.259				0.696			
Mn	0.656				0.014			
Mg	0.156				0.232			
Ca	0.004				0			
Sr	0				0			
Ba	1.763				0.939			
Na	4.366				4.012			
K	3.689				5.133			
Zr	0.024				0			
Nb	0.204				0.752			
Ta	0.001				0.003			

Note: The formula is calculated on the basis of Si + Al = 16.

hot-air blower (Armbruster 1986). Cell data were collected in steps of ca. 20 °C and the crystal was equilibrated for ca. 30 min at each temperature setting. After measurement at 200 °C the crystal was held at this temperature and an additional data set was collected up to θ = 25° to learn more about labuntsovite dehydration. However, being held for 72 hours at 200 °C led to a dramatic decrease of the cell volume from originally 1382 to 1367 Å^3. Thus the crystal had not obtained equilibrium and dehydration continued during data collection. This low-quality data set was only used to confirm loss of ca. 40% H_2O at W1 and W2. In addition, the Ba concentration on at the C site decreased significantly and new electron density appeared in the center of the structural channels. Furthermore, after this prolonged heat-treatment the originally sharp X-ray reflections became broadened and diffuse, smeared ca. 5° in ω direction (particularly *h*00 reflections), indicating strong increase in crystal tesselation.

The thermal-expansion data indicated the possibility of a phase transition at ca. –80 °C (see discussion section) and a second crystal (A2) from the same batch as A1 was structurally investigated at –160 and 22 °C.

Only diffraction data collected with an Enraf Nonius CAD4 diffractometer were used for structure refinement. These intensity data (subcell data defined by sharp reflections with c = 7.75 Å) were corrected for absorption by collecting empirical ψ-scans. Data reduction, including Lorentz and polarization correction, was performed with the SDP program package (Enraf Nonius 1982). Structure solution and refinement were performed with the programs XS and XL (Bruker AXS 1998) using neutral atom scattering factors. For experimental details see Table 2. Occupancies of all extraframework cations were refined for crystal B at 22 °C and A2 at –160 °C. The population of the H_2O molecule (OWC) forming the octahedral apices of the interstitial D octahedron was constrained to the D occupancy. The two symmetry-independent H_2O sites W1 and W2 were found to be split and each split position was 50% occupied. Refined populations of the –160 °C data (crystal A2) were transferred to the corresponding 22 °C refinement and fixed. Atomic coordinates, populations, and displacement parameters for crystal A2 (–160 and 22 °C) and crystal B are listed in Tables 3–5. Selected interatomic distances are summarized in Table 6.

To monitor diffuse scattering in both crystals (A2 and B1) additional diffraction data were collected with a MAR300 image plate using a quartz monochromator and a rotating Mo-anode as the X-ray source. The advantage of this machine is that diffraction data can be reconstructed into reciprocal layers (program XCAVATE by Estermann and Steurer 1998) allowing analysis of diffuse features (Figs. 1–4).

TABLE 2. Data collection and refinement parameters for labuntsovite-group minerals measured with a CAD4 diffractometer

Sample	A2 at –160 °C	A2 at 22 °C	B at 22 °C
Crystal size (mm)	0.10 × 0.25 × 0.45	0.10 × 0.25 × 0.45	0.13 × 0.15 × 0.40
space group	*C2/m*	*C2/m*	*C2/m*
a (Å)	14.2147(16)	14.2446(14)	14.237(3)
b (Å)	13.764(3)	13.7884(15)	13.768(3)
c (Å)	7.7574(12)	7.7798(9)	7.767(16)
β (°)	116.653(9)	116.709(8)	116.83(2)
θ max. (°)	35	35	30
hkl (min., max.)	$-22 \le h \le 21$	$-22 \le h \le 21$	$-20 \le h \le 18$
	$-1 \le k \le 22$	$-1 \le k \le 22$	$-1 \le k \le 19$
	$-1 \le l \le 12$	$-1 \le l \le 12$	$-1 \le l \le 10$
Scan type	1.5° ω + 0.35tanθ	1.5° ω + 0.35tanθ	1.5° ω + 0.35tanθ
Measured reflections	3854	3876	2642
Observed reflections ($I > 2\sigma I$)	2769	2708	1786
Unique reflections	3079	3099	2048
Number of parameters	154	147	153
R_{int} (%)	1.69	1.73	1.05
R_σ (%)	1.76	1.91	1.69
R_1 (%)	2.47	2.44	2.25
wR_2 (%)	6.87	6.86	6.37
GooF	1.107	1.086	1.131

TABLE 3A. Atomic coordinates, populations, and equivalent isotropic displacement parameters for labuntsovite-group mineral A2 at –160 °C

Atom	Population	*x*	*y*	*z*	B_{eq} (Å^2)
Ti1	1.040(3)	1/4	1/4	1/2	1.068(8)
Ti2	1.013(3)	0	0.22676(3)	1/2	1.083(6)
Si1	1	0.20835(3)	0.11018(3)	0.80434(6)	0.318(5)
Si2	1	0.32098(3)	0.11115(3)	0.25107(6)	0.346(5)
O1	1	0.08243(8)	0.11596(8)	0.6755(2)	0.53(1)
O2	1	0.10118(8)	0.22302(8)	0.3979(2)	0.56(1)
O3	1	0.42044(9)	0.18104(8)	0.3019(2)	0.65(1)
O4	1	0.26639(8)	0.12413(8)	0.3916(2)	0.52(1)
O5	1	0.3662(1)	0	0.2712(2)	0.51(2)
O6	1	0.23232(9)	0.12784(8)	0.0282(2)	0.59(1)
O7	1	0.2476(1)	0	0.7867(2)	0.45(2)
O8	1	0.27432(8)	0.18389(8)	0.7404(2)	0.46(1)
Ba (C)	0.453(1)	0.08723(5)	0	0.34250(5)	0.453(5)
OW (C)	0.493(3)	0.1098(6)	0	0.349(1)	1.5(2)
Mn (D)	0.493(3)	0	0	1/2	0.51(1)
K (B)	0.854(5)	0.42068(5)	0	0.70446(9)	1.22(1)
Na (B)	0.076(5)	0.4294(7)	0.0509(9)	0.731(1)	0.7(2)
Na (A)	0.473(4)	0.4134(1)	0.2629(1)	0.0116(3)	1.32(3)
W1	0.5	–0.0254(2)	0.1129(2)	–0.0059(4)	1.67(5)
W2	0.5	0.4732(2)	0.1469(2)	0.0095(4)	1.35(4)

TABLE 3B. Anisotropic displacement parameters U_{ij} for labuntsovite-group mineral A2 at –160 °C

Atom	U_{11}	U_{22}	U_{33}	U_{12}	U_{13}	U_{23}
Ti1	0.0323(3)	0.0052(2)	0.0103(2)	0.0063(1)	0.0160(2)	0.0034(1)
Ti2	0.0107(2)	0.0044(2)	0.0124(2)	0	–0.0070(1)	0
Si1	0.0040(2)	0.0038(2)	0.0036(2)	–0.0001(1)	0.0011(1)	0.0001(1)
Si2	0.0051(2)	0.0040(2)	0.0042(2)	–0.0004(1)	0.0022(1)	–0.0003(1)
O1	0.0047(4)	0.0065(4)	0.0073(4)	0.0003(3)	0.0013(3)	0.0009(3)
O2	0.0041(4)	0.0120(4)	0.0049(4)	0.0006(3)	0.0017(3)	–0.0001(3)
O3	0.0078(4)	0.0077(4)	0.0104(4)	–0.0035(3)	0.0053(3)	–0.0035(3)
O4	0.0080(4)	0.0073(4)	0.0060(4)	0.0011(3)	0.0045(3)	0.0004(3)
O5	0.0067(5)	0.0045(5)	0.0083(6)	0	0.0034(5)	0
O6	0.0090(4)	0.0088(4)	0.0034(4)	0.0010(3)	0.0018(3)	0.0000(3)
O7	0.0060(5)	0.0038(5)	0.0075(6)	0	0.0032(5)	0
O8	0.0057(4)	0.0060(4)	0.0054(4)	–0.0004(3)	0.0022(3)	0.0012(3)
Ba (C)	0.0056(2)	0.0066(1)	0.0047(1)	0	0.0021(1)	0
Mn (D)	0.0055(4)	0.0034(4)	0.0073(4)	0	0.0002(3)	0
K (B)	0.0106(3)	0.0269(5)	0.0085(3)	0	0.0041(2)	0
Na (A)	0.0119(7)	0.0113(7)	0.029(1)	–0.0011(5)	0.0108(6)	–0.0032(6)
W1	0.021(1)	0.033(1)	0.011(1)	–0.013(1)	0.009(1)	–0.004(1)
W2	0.013(1)	0.023(1)	0.016(1)	–0.0019(9)	0.0069(9)	0.000(1)

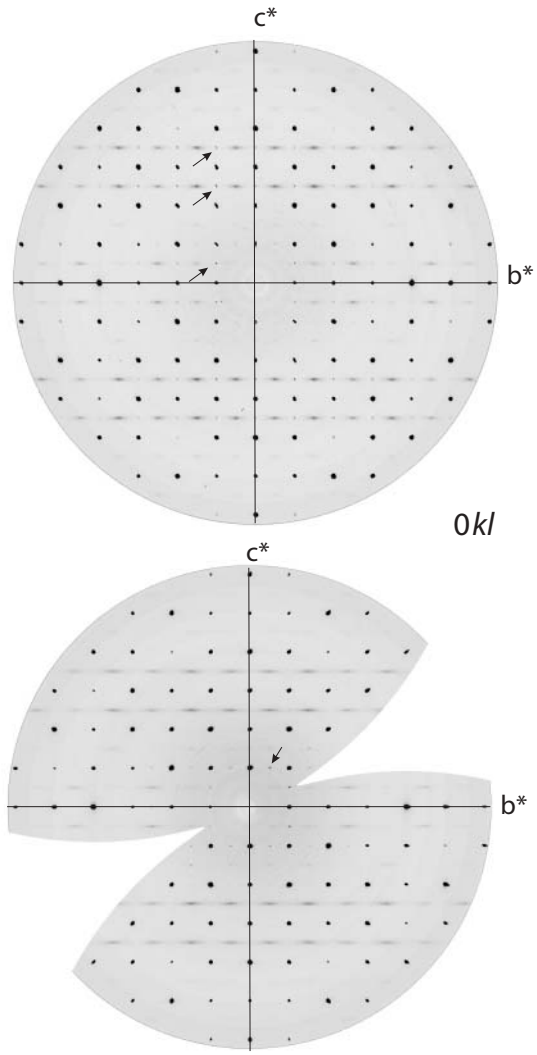

FIGURE 1. Reconstructed 0*kl* reciprocal space plots for crystals A2 and B displaying sharp X-ray reflections indicating a *C*2/*m* average structure with c = 7.75 Å and diffuse layers at $c^*/2$ intervals fulfilling conditions of an *I*-centered superlattice. Upper figure: Crystal A2 also displays weak but very sharp reflections within the diffuse layers (see arrows) indicating an additional superstructure of a *C*-centered lattice with c = 15.5 Å. Lower figure: Crystal B lacks evidence for this *C*-centered superlattice with c =15.5 Å but there are very few weak but sharp reflections originating from λ/2 diffraction of very strong reflections of doubled order. The effect of λ/2 diffraction has also been considered for crystal A2 but has been ruled out in particular for the high angle reflections with l = 5 and 7. The empty sectors are due to incomplete data collection.

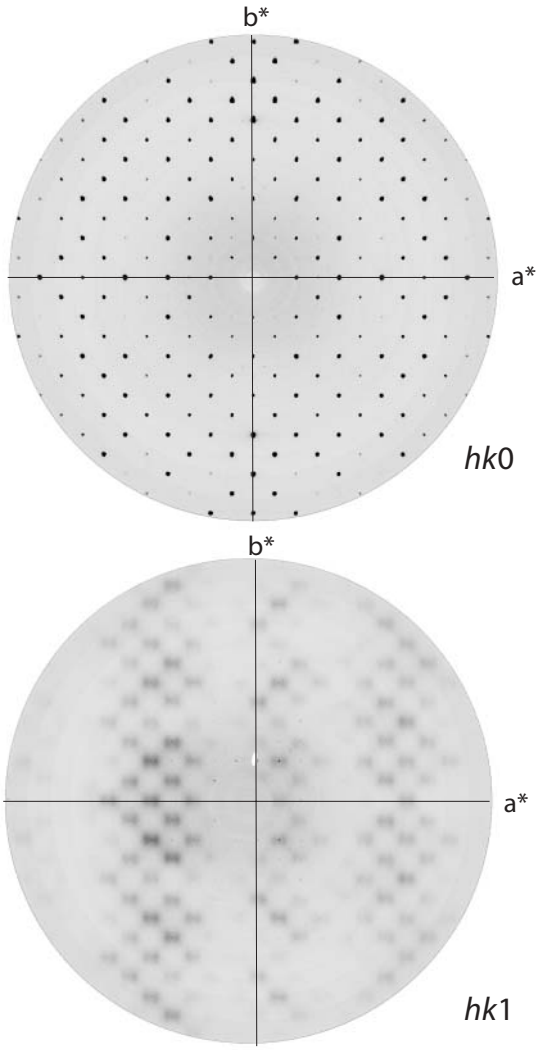

FIGURE 2. Reconstructed *hk*0 and *hk*1 reciprocal space plots for crystal B. Note that the *hk*0 reflections are all sharp whereas the *hk*1 reflections reveal a diffuse pattern where intensities are arranged in strings extending parallel to **b***.

THERMAL EXPANSION

Thermal expansion data collected between –160 and 200 °C indicate a possible phase transition at ca. –80 to –100 °C (Fig. 5). When crystal A was step-wise cooled from 22 to –160 °C, the β angle decreased up to –100 °C and then increased again. This unusual behavior is also reflected in the c parameter, which first significantly decreased and then remained constant between –80 and –160 °C. Comparison of coordinates, anisotropic displacement parameters (Tables 3 and 4), and bond lengths (Table 6) obtained from the –160 and 22 °C data sets did not provide insight to the nature of this transition. However, this is not surprising because our structural data only reflect the average structure and minor effects like changes in the network of hydrogen bonds cannot be resolved.

When heating the crystal from 22 °C to higher temperatures (Fig. 5), there is a rather isotropic expansion of all three axes until ca. 120 °C. From this temperature on thermal expansion increases rapidly (in particular along **a** and **c**) which is interpreted as being caused by strong thermal motion of loosely bound extraframework occupants (e.g., H_2O). Above ca. 150 °C the slope of expansion decreases again which is probably related to slow dehydration. Evidence for the dehydration could be found in structural data collected at 200 °C. Furthermore, the crystal held 72 h at 200 °C had a volume of 1382 $Å^3$ at the beginning, but after 72 h the volume decreased to 1367 $Å^3$ which is also

TABLE 4A. Atomic coordinates, populations, and equivalent isotropic displacement parameters for labuntsovite-group mineral A2 at 22 °C

Atom	Population	*x*	*y*	*z*	B_{eq} (Å^2)
Ti1	1.040	1/4	1/4	1/2	1.291(7)
Ti2	1.013	0	0.22749(3)	1/2	1.289(5)
Si1	1	0.20812(3)	0.11020(3)	0.80356(5)	0.493(5)
Si2	1	0.32038(3)	0.11124(3)	0.24992(5)	0.526(5)
O1	1	0.08239(8)	0.11665(7)	0.6755(2)	0.79(1)
O2	1	0.10108(8)	0.22393(8)	0.3979(2)	0.87(1)
O3	1	0.42024(8)	0.18042(8)	0.3028(2)	0.97(1)
O4	1	0.26511(8)	0.12486(8)	0.3884(2)	0.82(1)
O5	1	0.3647(1)	0	0.2705(2)	0.86(2)
O6	1	0.23313(9)	0.12821(8)	0.0271(1)	0.95(1)
O7	1	0.2464(1)	0	0.7858(2)	0.80(2)
O8	1	0.27392(8)	0.18286(7)	0.7384(1)	0.75(1)
Ba (C)	0.453	0.08730(4)	0	0.34257(5)	0.949(4)
OW (C)	0.493	0.1094(6)	0	0.346(1)	2.7(2)
Mn (D)	0.493	0	0	1/2	0.92(1)
K (B)	0.854	0.42052(6)	0	0.7032(1)	2.66(2)
Na (B)	0.076	0.4304(8)	0.0503(8)	0.729(2)	1.3(1)
Na (A)	0.473	0.4122(2)	0.2627(1)	0.0098(3)	2.29(3)
W1	0.5	–0.0249(3)	0.1128(3)	–0.0047(5)	2.55(5)
W2	0.5	0.4733(2)	0.1475(3)	0.0101(5)	2.34(5)

TABLE 4B. Anisotropic displacement parameters U_{ij} for labuntsovite-group mineral A2 at 22 °C

Atom	U_{11}	U_{22}	U_{33}	U_{12}	U_{13}	U_{23}
Ti1	0.0359(2)	0.0075(1)	0.0135(2)	0.0061(1)	0.0181(2)	0.0033(1)
Ti2	0.0131(2)	0.0064(1)	0.0152(2)	0	–0.0063(1)	0
Si1	0.0060(1)	0.0060(1)	0.0057(1)	–0.0001(1)	0.0016(1)	0.0005(1)
Si2	0.0076(2)	0.0060(2)	0.0065(1)	–0.0008(1)	0.0033(1)	–0.0007(1)
O1	0.0069(4)	0.0094(4)	0.0111(4)	0.0001(3)	0.0018(3)	0.0019(3)
O2	0.0066(4)	0.0170(4)	0.0095(4)	0.0002(3)	0.0038(3)	–0.0002(3)
O3	0.0118(4)	0.0114(4)	0.0155(4)	–0.0054(3)	0.0076(4)	–0.0051(3)
O4	0.0137(4)	0.0102(4)	0.0104(4)	0.0007(3)	0.0081(3)	–0.0003(3)
O5	0.0117(6)	0.0060(5)	0.0160(6)	0	0.0071(5)	0
O6	0.0132(4)	0.0150(4)	0.0065(4)	0.0017(3)	0.0031(3)	0.0000(3)
O7	0.0102(5)	0.0059(5)	0.0152(6)	0	0.0063(5)	0
O8	0.0095(4)	0.0097(4)	0.0092(4)	–0.0014(3)	0.0041(3)	0.0015(3)
Ba (C)	0.0118(2)	0.0134(1)	0.0109(1)	0	0.0051(1)	0
Mn (D)	0.0104(3)	0.0063(3)	0.0122(3)	0	–0.0004(3)	0
K (B)	0.0234(3)	0.0580(7)	0.0187(3)	0	0.0086(2)	0
Na (A)	0.0213(8)	0.0222(8)	0.046(1)	–0.0016(6)	0.0177(8)	–0.0047(8)
W1	0.031(2)	0.047(2)	0.022(1)	–0.014(1)	0.016(2)	–0.006(1)
W2	0.023(1)	0.040(2)	0.029(1)	–0.002(1)	0.013(1)	–0.002(1)

TABLE 5A. Atomic coordinates, populations, and equivalent isotropic displacement parameters for labuntsovite-group mineral B at 22 °C

Atom	Population	*x*	*y*	*z*	B_{eq} (Å^2)
Ti1	1.022(3)	1/4	1/4	1/2	1.08(1)
Ti2	1.016(3)	0	0.22712(3)	1/2	1.113(8)
Si1	1	0.20816(4)	0.10996(3)	0.80316(6)	0.478(6)
Si2	1	0.31987(4)	0.11131(3)	0.24992(6)	0.509(7)
O1	1	0.08209(9)	0.11590(9)	0.6736(2)	0.80(2)
O2	1	0.10065(9)	0.22441(9)	0.3970(2)	0.71(2)
O3	1	0.4199(1)	0.18084(9)	0.3030(2)	0.93(2)
O4	1	0.2652(1)	0.12522(9)	0.3893(2)	0.79(2)
O5	1	0.3645(1)	0	0.2714(3)	0.83(3)
O6	1	0.2326(1)	0.1282(1)	1.0265(2)	0.90(2)
O7	1	0.2474(1)	0	0.7868(3)	0.81(3)
O8	1	0.27370(9)	0.18328(9)	0.7385(2)	0.75(2)
Ba (C)	0.380(1)	0.08538(4)	0	0.3423(1)	1.05(1)
OW (C)	0.460(3)	0.1043(8)	0	0.347(2)	2.37
Fe (D)	0.460(3)	0	0	1/2	0.91(3)
K (B)	0.89(2)	0.41995(9)	0	0.7027(2)	2.35(7)
Na (B)	0.07(2)	0.429(2)	0.042(2)	0.718(3)	0.5(4)
Na (A)	0.485(5)	0.4133(2)	0.2624(1)	0.0103(3)	2.05(4)
W1	1	–0.0248(3)	0.1138(3)	–0.0061(7)	2.47(7)
W2	1	0.4733(2)	0.1465(3)	0.0102(5)	1.92(5)

TABLE 5B. Anisotropic displacement parameters U_{ij} for labuntsovite-group mineral B at 22 °C

Atom	U_{11}	U_{22}	U_{33}	U_{12}	U_{13}	U_{23}
Ti1	0.0301(3)	0.0058(2)	0.0116(2)	0.0054(2)	0.0153(2)	0.0027(2)
Ti2	0.0115(2)	0.0046(2)	0.0137(2)	0	–0.0054(2)	0
Si1	0.0063(2)	0.0050(2)	0.0062(2)	–0.0003(1)	0.0022(2)	0.0005(1)
Si2	0.0075(2)	0.0052(2)	0.0069(2)	–0.0007(2)	0.0034(2)	–0.0007(2)
O1	0.0072(5)	0.0091(5)	0.0114(6)	0.0003(4)	0.0018(5)	0.0026(4)
O2	0.0051(5)	0.0132(6)	0.0092(5)	–0.0003(4)	0.0036(4)	–0.0006(4)
O3	0.0122(6)	0.0102(6)	0.0149(6)	–0.0049(5)	0.0077(5)	–0.0045(5)
O4	0.0126(5)	0.0084(5)	0.0113(5)	0.0006(4)	0.0074(5)	–0.0005(4)
O5	0.0109(8)	0.0057(7)	0.0156(8)	0	0.0065(7)	0
O6	0.0125(6)	0.0132(6)	0.0072(5)	0.0011(5)	0.0033(5)	–0.0003(4)
O7	0.0108(8)	0.0051(7)	0.0166(9)	0	0.0078(7)	0
O8	0.0095(5)	0.0094(5)	0.0097(5)	–0.0011(4)	0.0045(4)	0.0024(4)
Ba (C)	0.0128(3)	0.0138(2)	0.0137(2)	0	0.0063(2)	0
Fe (D)	0.0095(6)	0.0049(6)	0.0130(6)	0	–0.0015(5)	0
K (B)	0.0231(4)	0.047(3)	0.0185(4)	0	0.0088(3)	0
Na (A)	0.021(1)	0.021(1)	0.040(1)	0.0001(7)	0.0169(9)	–0.0027(8)
W1	0.029(2)	0.043(2)	0.026(2)	–0.011(1)	0.016(2)	–0.005(2)
W1	0.019(2)	0.031(2)	0.024(1)	–0.002(1)	0.011(1)	–0.002(1)

characteristic of slow H_2O release. When the crystal was cooled to 22 °C the cell volume further decreased to 1356 Å^3 associated with crystal tessellation derived from smearing of originally sharp reflections. Before heating the same crystal at 22 °C had a volume of 1368 Å^3.

MODELING OF SUPERSTRUCTURES

Structure modeling was guided by comparison of the diffuse intensity distribution in the reciprocal $l = 2n + 1$ layers (odd layers for a doubled cell with c = 15.5 Å) with the intensity distribution in the corresponding layers calculated from an ordered structural model. The model structure was obtained with the following procedure: (1) Coordinates of the –160 °C data set of crystal A2 were transformed to $P1$ symmetry. All symmetry operations ($^1/_2$, $^1/_2$, 0; $-x, -y, -z$; $x, -y, z$; $-x, y, -z$) were removed and each atom in the unit cell was treated as symmetry independent. (2) This $P1$ cell with c = 7.75 Å was transformed to a cell with a doubled c-axis of 15.5 Å. The first half of the atomic coordinates was obtained by dividing the z-coordinates by 2 ($z_{new1} = z_{old}/2$) and the second half of the structure was derived by adding positions with $z_{new2} = z_{new1} + {}^1/_2$. (3) In the course of the modeling all positions of the octahedral-tetrahedral framework remained fixed and the different models were only distinct in the distribution of extraframework ions and H_2O molecules. (4) For structure modeling an idealized chemical composition was assumed. Selection of extraframework occupants from among those obtained from the disordered average structure with c = 7.75 Å was guided by reasonable distances to neighboring channel occupants. (5) Atomic coordinates and occupancies of the trial models were used for structure factor (intensity) calculation. (6) The calculated diffraction pattern was displayed with reciprocal space plots created with the XPREP program in the SHEXTL package (Bruker AXS 1998). (7) If a model was found to be in good agreement with the intensity distribution of the diffuse layers, the calculated structure factors were used to find the true symmetry of the model and atomic coordinates for the respective space group were obtained by structure solution and refinement based on the calculated structure factors of the original $P1$ model.

Inspection of the observed superstructure reflections in the diffuse odd l-layers (Figs. 1 and 3) indicated that two different sets of superstructure reflections had to be considered. (1) Weak but extremely sharp reflections fulfilling C-centering. These C-type reflections were only observed in crystal A but not in crystal B. (2) Very diffuse reflections streaked along **a*** fulfilling I-cen-

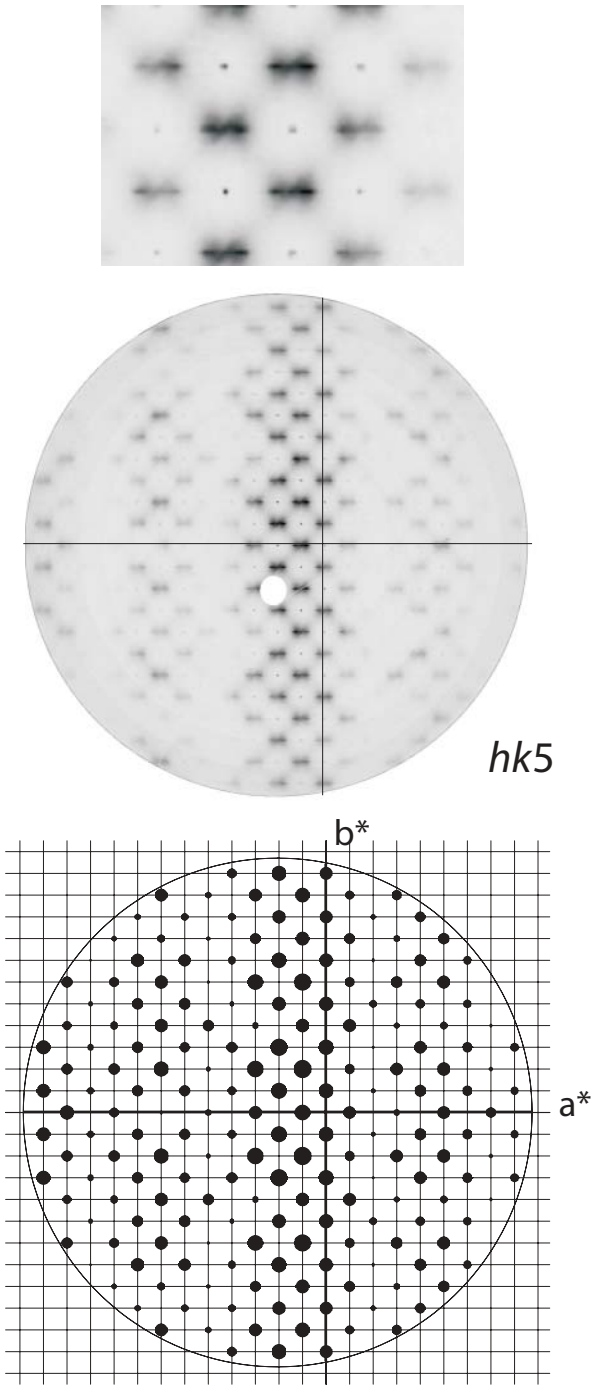

FIGURE 3. Observation and interpretation of the reconstructed *hk*5 reciprocal space layer of crystal A2. Upper figure: Close up of an area of the *hk*5 layer showing diffuse reflections of the *I*-centered superlattice and sharp reflections referring to the *C*-centered superlattice. Middle figure: observed *hk*5 layer. The hole in the lower left quadrant represents an area of missing data. Lower figure: Calculated Bragg *hk*5 layer obtained for a model structure with space group *C*2/*m* and c = 15.5 Å. For details consult the text. The calculated diffraction pattern only explains the diffuse reflections related to the *I*-centered lattice. The size of the black spots correlates with the calculated intensities.

TABLE 6. Selected interatomic distances in labuntsovite-group minerals

			A2 –160 °C	A2 22 °C	B 22 °C
Ti1	–	Distance			
	O2	×2	1.9331(11)	1.9354	1.9364(13)
	O8	×2	1.9610(11)	1.9611	1.956(13)
	O4	×2	1.9845(11)	1.9864	1.9767(13)
Ti2	–	Distance			
	O3	×2	1.9213(11)	1.9209	1.9164(14)
	O2	×2	1.9292(11)	1.9323	1.9315(12)
	O1	×2	2.0299(11)	2.0338	2.0264(13)
Si1	–	Distance			
	O8	×1	1.6039(11)	1.6018	1.6015(13)
	O1	×1	1.6137(11)	1.6137	1.6158(14)
	O6	×1	1.6312(12)	1.6296	1.6275(14)
	O7	×1	1.6427(7)	1.6414	1.6383(9)
Si2	–	Distance			
	O3	×1	1.6060(11)	1.6051	1.6075(13)
	O4	×1	1.6068(11)	1.6055	1.6038(14)
	O6	×1	1.6354(11)	1.6335	1.6322(14)
	O5	×1	1.6395(7)	1.6388	1.6385(8)
Ba (C)	–	Distance			
	Mn6	×1	2.0951(6)	2.1013	2.0786(7)
	W1**	×2	2.819(3)	2.831	2.825(4)
	O1	×2	2.8426(12)	2.8539	2.8248(14)
	W1*	×2	2.899(3)	2.897	2.900(5)
	O4	×2	2.9461(12)	2.9486	2.9696(14)
	O1	×2	3.0631(12)	3.0761	3.0460(14)
	O2	×2	3.0935(13)	3.1116	3.1130(15)
Mn, Fe (D)	–	Distance			
	O1	×4	2.0838(11)	2.0947	2.0754(13)
	Ba	×2	2.0951(6)	2.1013	2.0786(8)
	OW	×2	2.333(7)	2.352	2.283(11)
K (B)	–	Distance			
	Na (B)	×2	0.725(13)	0.719	0.59(4)
	O7	×1	2.8047(16)	2.827	2.813(2)
	W2	×2	2.878(3)	2.892	2.880(4)
	W2	×2	2.943(3)	2.964	2.951(4)
	O5	×1	2.9494(16)	2.9733	2.983(2)
	O4	×2	2.9738(12)	2.9983	2.9850(17)
	O5	×1	3.0923(17)	3.0918	3.075(2)
Na (B)	–	Distance			
	K (B)	×1	0.725(13)	0.719	0.50(4)
	Na (B)	×1	1.40(2)	1.388	1.15(7)
	W2	×1	2.28(1)	2.298	2.41(4)
	W2	×1	2.37(1)	2.394	2.51(3)
	O4	×1	2.801(9)	2.833	2.81(1)
	O3	×1	2.885(10)	2.8789	2.94(3)
	O7	×1	2.890(9)	2.928	2.929(18)
	O8	×1	2.891(10)	2.907	2.999(18)
	O5	×1	2.997(9)	3.000	2.966(12)
Na (A)	–	Distance			
	W2	×1	1.812(3)	1.811	1.810(4)
	W1	×1	1.950(4)	1.964	1.950(4)
	W2	×1	2.327(3)	2.331	2.327(4)
	W1	×1	2.349(3)	3.364	2.340(4)
	O8	×1	2.406(2)	2.410	2.409(3)
	O6	×1	2.465(2)	2.469	2.475(2)
	O3	×1	2.480(2)	2.502	2.500(3)
	Na	×1	2.548(3)	2.574	2.545(4)
	O1	×1	2.923(2)	2.933	2.949(3)
	O2	×1	2.994(2)	3.015	2.990(3)

Notes: Underlined positions display unreasonable distances and are due to positional disorder. Positions flagged with one or two asterisks are also disordered and only one of them is occupied.

tering. These *I*-type reflections are dominant in A and B crystals. All superstructure reflections in *hkn* layers (Figs. 2–4) were found to be arranged in broad strings extending parallel to **b***. The string to string separation along **a*** is ca. 0.422 Å^{-1}.

In the average-structure model with c = 7.75 Å there is a twofold axis running through the structural channels, which prevents an ordered arrangement of extraframework occupants. However, if the c parameter is doubled there is no rotation axis running parallel to the structural channel; thus order within a single channel becomes possible.

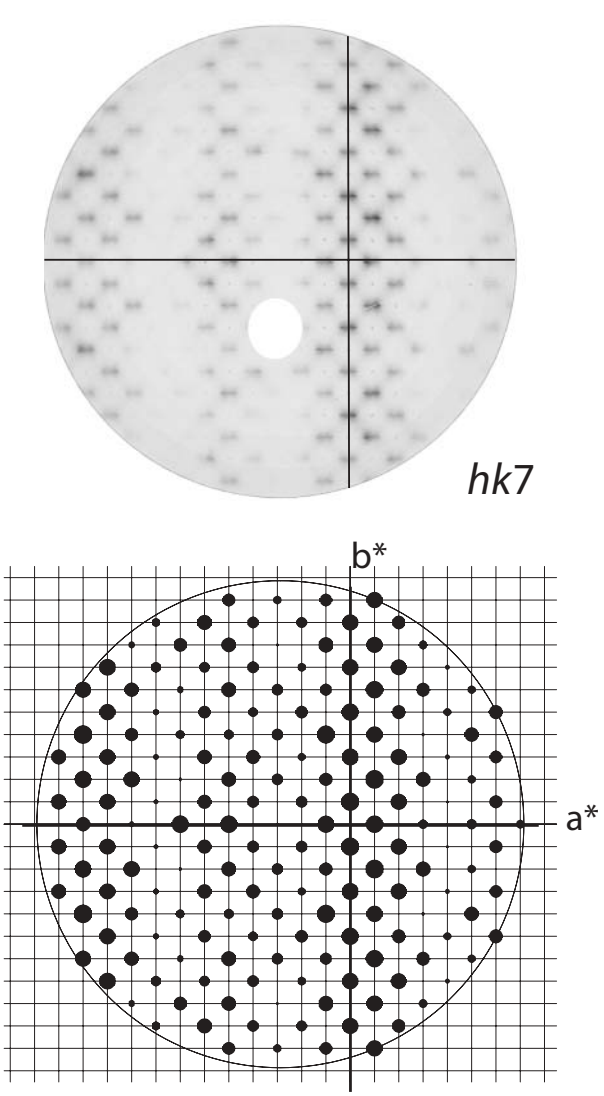

FIGURE 4. Observation and interpretation of the reconstructed *hk*7 reciprocal space layer of crystal A2. Compare with Figure 3.

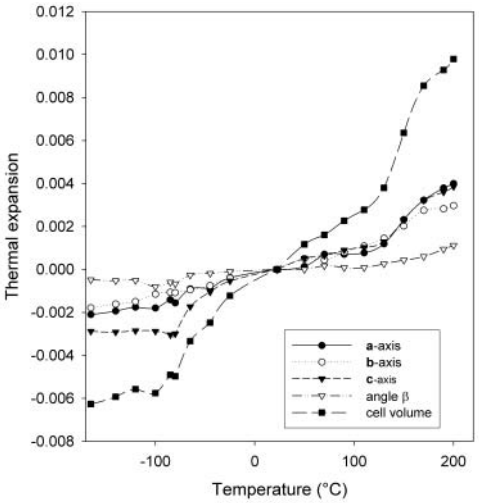

FIGURE 5. Thermal expansion of sample A determined from single-crystal X-ray data between –160 and 200 °C. The plotted parameters are $(y_T - y_{22\,°C})/y_{22\,°C}$, where y represents the **a**, **b**, and **c** axes, the cell volume, and the β angle. For the discussion see the text. The size of the symbols is significantly larger than the associated standard deviations for each point.

The average structure

Rastsvetaeva et al. (1997) refined the structure of a labuntsovite mineral with similar composition to our crystal A and their assignment of extraframework ion and H_2O molecules is consistent with our study. Unfortunately Rastsvetaeva et al. (1997) only provided isotropic displacement parameters which obscures some important structural details. In their refinement the channel H_2O molecules are placed on the twofold axis and display very high B values of 9.5 and 6.6 Å^2. In our study these H_2O molecules are clearly displaced from the twofold axis (separated from each other by 0.7 and 0.8 Å, respectively) and at 22 °C the corresponding B_{eq} values fall to 2.3 and 2.6 Å^2. As shown below disorder caused by the twofold axis is essential for understanding the "true" structure of the labuntsovite-group minerals.

In both refinements (sample A and B) the electron density at the Ti1 and Ti2 sites was refined using Ti (22 electrons) as a dummy atom (representing possible Ti, Nb, Mg) yielding an average of 22.6(1) e/Å^3 (sample A) and 22.5(1) e/Å^3 (sample B). This is rather surprising as sample B has ca. 10% Nb replacing Ti. The relatively low electron density in sample B can only be explained by balancing the Nb (41 electrons) concentration by Mg (12 electrons). According to electron-microprobe analyses (Table 1), the Ti1 and Ti2 sites (8 pfu) must be occupied by 7.425 Ti + 0.024 Zr + 0.204 Nb + 0.001 Ta + 0.156 Mg + 0.19 Fe = 8 (sample A) and 6.951 Ti + 0.752 Nb + 0.003 Ta + 0.232 Mg + 0.062 Fe = 8 (sample B). These cation assignments yield predicted mean electron densities of 22.4 and 23.5 electrons. In sample A 0.656 Mn + 0.069 Fe = 0.73 pfu and in sample B 0.634 Fe + 0.014 Mn = 0.65 pfu remain for the octahedral D site. These values are significantly lower than those determined in the structure refinement of 0.99 pfu (12.3 e/Å^3) and 0.92 pfu (11.5 e/Å^3), respectively. The poor agreement between refined D-site occupancies and electron-microprobe analyses may be explained by the following arguments. (1) The structure model is flawed as it is characteristic of an average structure without considering diffuse superstructure reflections; (2) Both crystals studied are chemically strongly zoned; (3) The occupancies of all heavy atoms (Ti sites, C site, D site) in the structure were refined. Thus there are pronounced correlations in the refinement model, e.g., among occupancies and the scale factor.

For an ideal lemmleinite-Ba composition there are 4 Na pfu and 4 K pfu. Sample A has 4.366 Na and 3.689 K pfu, thus some Na is replacing K. This could also be confirmed by the structure refinement where we observed satellite positions around K with significantly shorter distances to the coordinating H_2O molecule (W2). With the satellite positions assigned to Na the structure refinement yielded 4.4 Na pfu and 3.4 K pfu. In addition, electron microprobe analyses suggest that the C site is occupied by 1.76 Ba pfu, which is confirmed by the site occupancy refinement converging at 1.81 Ba pfu. Probably minor K is also substituting at C. Sample B has excess K of 5.133 pfu indicating that K is also

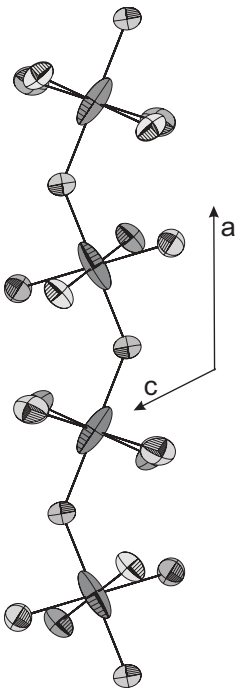

FIGURE 6. Chain of corner-connected TiO_6 octahedra extending parallel to **a** displayed with probability ellipsoids (arbitrary scale) representing anisotropic displacement parameters (crystal A2 at 22 °C). The smearing of Ti within a rather rigid octahedron is temperature independent and represents a characteristic feature of the average structures (c = 7.75 Å) for crystals A and B. Our interpretations assumes for the superstructure variable out-of-center displacement of Ti yielding for the average structure the observed overlay where Ti is smeared out along a vector defined by corner-connecting octahedral apices.

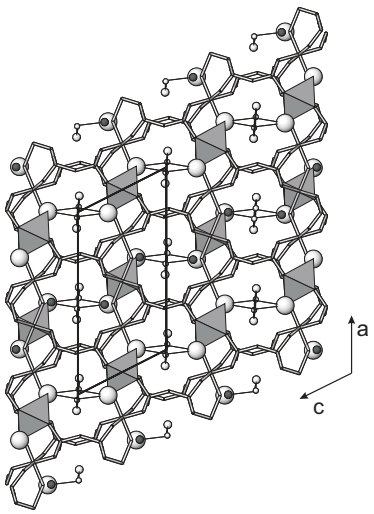

FIGURE 7. Representation of the *C*2/*m* average structure with c = 7.75 Å for crystals A and B. The porous titanosilicate framework is displayed by a bond model where TiO_6 octahedra form corner-connecting chains parallel to **a,** crosslinked approximately parallel to **c** by four-membered rings of tetrahedra. The gray-shaded octahedra represent interstitial D sites (Fe, Mn, Mg) edge-connecting adjacent TiO_6 chains along **b**. The octahedral D apices extending into the structural channel are formed by H_2O molecules. The partially occupied D sites are disordered with C sites (Ba, K) (represented by white large spheres) situated almost at the same position as the H_2O molecules completing the D coordination. At the same x, z coordinates but on a different y-level as the C site are the K-occupied B sites (dark gray sphere). The extraframework occupants (small spheres: H_2O, intermediate spheres: Na) in the center of the channels are disordered by a twofold axis and only one-half can be simultaneously occupied. The H_2O molecules W1 and W2 are overlain but occupy different levels along **b**. W1 bonds to Ba (C site) and Na whereas W2 bonds to K (B site) and Na.

partially replacing Ba at the C site. If 1.133 K and 0.939 Ba are occupying the C site sample B has to be considered a solid-solution member between lemmleinite-K and lemmleinite-Ba. The prevalence of K over Ba, however, suggests a formal definition of this sample as lemmleinite-K. The structure refinement using Ba as a dummy atom (representing Ba, K, and vacancies) for the C site yielded 1.55 Ba pfu, which corresponds to 21.7 e/Å^3 at C. Transformation of the analyzed Ba and K concentrations to average electron density yields 18.5 e/ Å^3. The discrepancy of ca. 3 e/Å^3 may be explained by the strong Ba variation in sample B (Table 1) and by the arguments stated above for the poor agreement between analyzed and refined D-site occupancies.

Anion order, Ti displacement, and extraframework arrangement

If we consider the idealized formulas of labuntsovite $Na_4K_4D_2Ti_8(Si_4O_{12})_4(O,OH)_8 \cdot 12H_2O$ (D = Mn, Fe, Mg) and lemmleinite-Ba $Na_4K_4Ba_2Ti_8(Si_4O_{12})_4(O,OH)_8 \cdot 8H_2O$ there are 108 positive charges pfu which is in good agreement with the 108.5$^+$ obtained for samples A and B if all iron is calculated as Fe^{2+} and the formula is normalized to Si + Al = 16. In an idealized formula 96 positive charges belong to the tetrahedral-octahedral framework and the remaining 12 come from the extraframework ions. For charge balance there are 48 O anions bonded to Si and an additional 8 connecting TiO_6 octahedra to form chains along **a.** To obtain a charge-balanced formula these Ti-connecting O sites (O2 in the c = 7.75 Å average structure) must be 50% occupied by O and 50% by OH. The formal bond strength of O2 is 2 × 4/6 = 1.333. All other framework O sites connect either two SiO_4 tetrahedra or link two TiO_6 octahedra to one SiO_4 tetrahedron and may thus be excluded as potential OH sites. In previous structural studies a corresponding position was also interpreted as an OH site (Rastsvetaeva et al. 1997, 1998).

If anisotropic displacement parameters at –160 and +22 °C are inspected (Tables 3 and 4) all atoms show a normal trend (expansion with increasing temperature) except the Ti1 and Ti2 sites which display a strong temperature-independent "smearing" parallel to the O2-O2 apices of the octahedron (Fig. 6). This anisotropy is interpreted as static disorder of Ti within rather rigid octahedra and must be related to the mixed OH and O occupancy of the O2 site in the average structure. Furthermore, Ti as a d^0 transition element cation generally prefers an octahedral out-of-center displacement interpreted as a second-order Jahn-Teller effect (Kunz and Brown 1995). We have also tested a model where the strongly anisotropic Ti1 and Ti2 positions are displaced from the special positions and split into two sites refined with isotropic displacement parameters. In such models both split Ti sites are separated by only 0.30 Å leading for crystal A2 (–160 °C) to the following Ti1-O distances: Ti1-O2 = 1.783(1) and 2.085(11) Å, Ti1-O8 = 1.952(1) and 1.983(1) Å, Ti1-O4 = 1.973(1) and 2.008(1) Å. For Ti2, the following Ti2-O distances were obtained: Ti2-O2 = 1.781 and 2.079(1), Ti2-O3 = 1.897(1) and 1.958(2) Å, Ti2-O1 = 2.020(1) and 2.051(1) Å. Most important, such models with split Ti positions did not lead to a significant improvement of the refinement quality. Furthermore, changing the refinement model did not influence the occupancies

of the atomic sites.

In our refinements of the average structures Ba at the C site also bonds to O2 (Fig. 7) and it is suggested that in the "true structure" Ba is only bonded to those O2 sites occupied by O and not to those occupied by OH. Thus there is a strong dependence between OH distribution in the framework and extraframework cation arrangement and vice versa. In minerals of idealized labuntsovite-subgroup composition $Na_4K_4D_2Ti_8(Si_4O_{12})_4(O, OH)_8 \cdot 12H_2O$ (D = Mn, Fe, Mg) there are no extraframework cations bonded to O2. However, the chemical data compiled by Chukanov et al. (1999) indicate that lemmleinite-labuntsovite solid solution members with low occupancy of the C site have decreased sums of cation charges thus O2 may be more than 50% occupied by OH in these cases.

There are other crystal-chemical limitations which help our understanding of superstructure formation. The C site (Ba) bonds to two O2 positions which must be occupied by O (not OH) which leads to the limiting value of 2 Ba pfu. In our two structure refinements Ba amounts to 1.71 (sample A) and 1.55 pfu (sample B). Furthermore, the highest Ba content analyzed by Chukanov et al. (1999) is 2.08 Ba pfu. In the average structure the C site is only less than 50% occupied which leads to the question of why a structure with full Ba occupancy (4 Ba pfu) does obviously not exist, although charge balance could be obtained by only O at O2. The answer to this question is found in the space requirements of Ba and its H_2O ligands in the channels of the structure. The average structure comprises two channels pfu along **b** and each channel can only host one Ba apfu.

Ba at the C site is attached to the wall of the channel and the coordinating H_2O molecules (W1) extend into the structural channels. In the average structure partially occupied C and W1 positions occur on opposite channel walls (Fig. 7). Each Ba bonds to two W1 H_2O molecules with a bonding distance of ca. 2.9 Å. However, the two H_2O molecules, bonding to the channel adjacent Ba sites, are disordered and split into two subsites each (half occupied). We interpret the W1 disorder to the fact that each subsite bonds to only one individual Ba site on opposite channel walls. If W1 is erroneously placed on the twofold axis (Rastsvetaeva et al. 1997) adjacent Ba positions share the same H_2O molecule, which is additionally bonded to Na. The hypothesis of a H_2O molecule (W1) bonded to two adjacent Ba sites and to one Na site can be rejected because such a highly coordinated H_2O molecule should display rather long W1-Ba and W1-Na distances. In contrast, the observed corresponding distances are among the shortest distances to Ba and Na (Table 6).

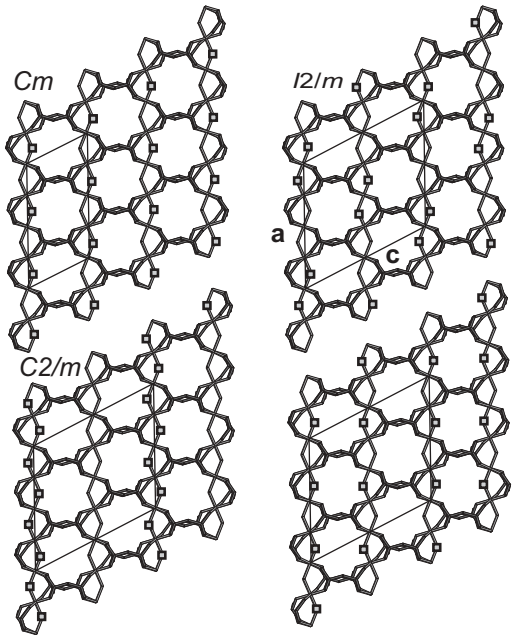

FIGURE 8. The titanosilicate framework of the labuntsovite-group minerals, displayed as in Figure 6. In addition, the OH sites, occupying 50% of the chain-forming octahedral apices, are marked by squares. The variable arrangement of OH groups leads to different superstructures. In addition, it is assumed that the C sites (Ba, K) close to OH groups are vacant. Space requirements of C cations and their coordinated H_2O ligands allow occupation of only one C site per channel. Upper left: Octahedral chains characterized by alternating apical OH and O sites yielding *Cm* symmetry with $c = 7.75$ Å. Upper right: Octahedral chains characterized by pairs of alternating apical OH and O sites yielding *I*2/*m* symmetry with $c = 15.5$ Å. Lower left: Alternating octahedral chains where all apices are either occupied by OH or O yielding *C*/2*m* symmetry with $c = 15.5$ Å. Lower right: Alternating OH and O sites for a $c = 15.5$ Å model. This model has to be rejected because it leads to doubly occupied and unoccupied channels.

The superstructures

If we obey the spatial limitations and model a structure with an ordered arrangement of 50% O and 50% OH at O2 where Ba only bonds to O-occupied O2 sites, we obtain several possible solutions (Fig. 8): (1) A structure of *Cm* space-group symmetry with $c = 7.75$ Å. This ideal structure has the advantage that each Ti has one OH and one O apex enhancing the Ti out-of-center distortion (Kunz and Brown 1995). Any deviation from Ba <

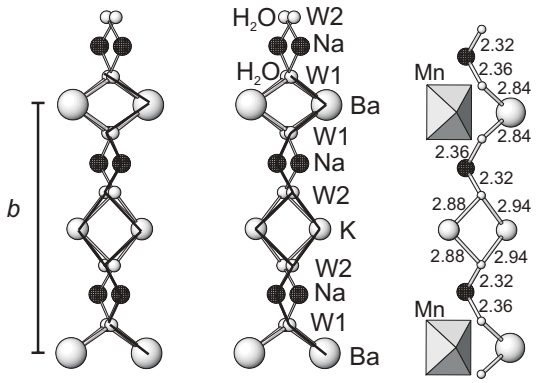

FIGURE 9. Channel occupants of the lemmleinite- and labuntsovite-subgroup minerals. In the average structure all occupants, except K at the B site, can only be half-occupied. Depending on which of the disordered Na sites is locally occupied, two different ordered arrangements can be predicted based on appropriate bonding distances. Left: Only the Na sites on the right are occupied. Middle: Only the Na sites on the left are occupied. Right: Modeled structure with *I*2/*m* symmetry leading to very good agreement with the observed diffuse reflections. In addition, octahedral D sites adjacent to the C sites are displayed. For agreement with the observed diffuse scattering see Figures 3 and 4. The numbers represent interatomic distances (Å).

TABLE 7A. Predicted ordered structures: *Cm* model for lemmleinite-Ba with $c = 7.75$ Å

Atom	*x*	*y*	*z*
Ti1	0.2500	0.2500	0.5000
Ti2	0.0000	0.2267	0.5000
Si1	0.2084	0.1102	0.8043
Si1′	–0.2084	0.1102	–0.8043
Si2	0.3210	0.1111	0.2511
Si2′	–0.3210	0.1111	–0.2511
O1	0.0824	0.1160	0.6755
O1′	–0.0824	0.1160	–0.6755
O2	0.1012	0.2230	0.3922
O2′	–0.1012	0.2230	–0.3922
O3	0.4204	0.1810	0.3019
O3′	–0.4204	0.1810	–0.3019
O4	0.26640	0.1241	0.3916
O4′	–0.26640	0.1241	–0.3916
O5	0.3662	0	0.2712
O5′	–0.3662	0	–0.2712
O6	0.2323	0.1278	0.0282
O6′	–0.2323	0.1278	–0.0282
O7	0.2476	0	0.7867
O7′	–0.2476	0	–0.7867
O8	0.2743	0.1839	0.7404
O8′	–0.2743	0.1839	–0.7404
Ba (C)	0.0872	0	0.3425
K (B)	0.4207	0	0.7045
K′ (B)	–0.4207	0	–0.7045
Na (A)	–0.4134	0.2629	–0.0012
W1	–0.0254	0.1129	–0.0059
W2	0.4732	0.1469	0.0095
(Na′ (A))	–0.4134	0.2629	0.0012
(W1′)	0.0254	0.1129	0.0059
(W2′)	–0.4732	0.1469	–0.0095

Note: Underlined positions are alternative sites also leading to reasonable interatomic distances.

TABLE 7B. Best model for the *I*2/*m* structure $c = 15.5$ Å

Atom	*x*	*y*	*z*
Ti1	0.25000	0.25000	0.50000
Ti2	0	0.226788	1/2
Ti2′	1/2	0.273212	1/2
Si1	0.20840	–0.11019	0.65220
Si1′	0.70840	0.61019	0.65220
Si2	0.17900	0.38890	0.62450
Si2′	0.32100	0.11110	0.37550
O1	–0.08239	0.11602	0.41232
O1′	0.58239	0.61602	0.58768
O2	0.60118	0.27703	0.44901
O2′	0.10118	0.22297	0.44901
O3	–0.07959	0.31889	0.40100
O3′	0.42041	0.18111	0.40100
O4	0.23360	0.37578	0.55420
O4′	0.26640	0.12422	0.44580
O5	0.13378	1/2	0.61440
O5′	0.36622	0	0.38560
O6	0.26770	0.37210	0.73589
O6′	0.23230	0.12790	0.26411
O7	0.24768	0	0.64336
O7′	0.74768	1/2	0.64336
O8	0.77440	0.68389	0.62020
O8′	0.27440	–0.18389	0.62020
Ba (C)	0.08710	0	0.42120
OWC	0.39088	1/2	0.57539
Mn (D)	1/2	1/2	1/2
K (B)	0.42070	0	0.60219
K′(B)	–0.0793	1/2	0.60219
Na (A)	0.41340	–0.26291	0.75580
W1	0.02540	0.11281	0.25149
W2	0.52682	–0.14701	0.74534

2 pfu and OH < 4 pfu will lead to stacking faults causing a *C*2/*m* average structure. (2) A structure of *I*2/m symmetry with doubled *c* dimension of 15.5 Å. This structure is characterized by Ti octahedra with the following O2-O2 apices along **a**: O-Ti-O-Ti-OH-Ti-OH-Ti-O....(3) A structure of *C*2/*m* symmetry with a doubled *c* parameter of 15.5 Å. This structure has adjacent chains of TiO_6 octahedra, which have either only OH or only O at the corner-connecting O2 positions. The latter two structures have the disadvantage that the Ti out-of-center distortion is not enhanced as in the first one. A structure with doubled *c* dimension and alternating OH,O positions along the octahedral chains (Fig. 8) is not possible because it would lead to two Ba atoms in one channel, which contradicts the steric constraints.

Model of a *Cm* structure with $c = 7.75$ Å

Using the average *C*2/*m* structure as a reference (crystal A, –160 °C data), there are always pairs of H_2O—extraframework cation distances where one distance is reasonable and the other is too short. The pair-wise appearance is due to the disorder caused by the twofold axis. If we now select only those extraframework sites yielding reasonable distances, we obtain a structure with ordered channel occupants (Table 7a). This model describes very well a hypothetical lemmleinite-Ba end-member $Na_4K_4Ba_2Ti_8(Si_4O_{12})_4O_4(OH)_4{\cdot}8H_2O$ but it fails as soon as additional octahedral cations at the D (Mn, Fe, Mg) sites have to be considered. If we introduce a D site (at 0, 0, 1/2) in this ordered structure, D sites are also generated close (ca. 2 Å) to the Ba positions. This model cannot explain the diffuse superstructure features because it has $c = 7.75$ Å.

Model of a *I*2/*m* structure with $c = 15.5$ Å

The modeled composition of this idealized superstructure is $Na_4K_4Ba_2MnTi_8(Si_4O_{12})_4(O,OH)_8{\cdot}10H_2O$. All extraframework cations are fully occupied and completely ordered and display reasonable distances to coordinating H_2O molecules and framework O atom sites (Fig. 9). This model (Table 7b) gives the best qualitative agreement between observed intensity of diffuse $l = 2n + 1$ layers and calculated structure factors (Figs. 3 and 4). There are actually two possible models distinguished only by the Na and H_2O arrangements in the channels (Fig. 9). In the first model Na, W1, and W2 are occupied whereas in the second model Na', W1', and W2' are fully occupied. However, only the first model is in agreement with the intensity distribution within the diffuse layers. A shortcoming of this model is the partly disordered arrangement of OH anions. For complete OH, O order at O2 (OH) and O2' (O) we obtain the formula $Na_4K_4Ba_2MnTi_8(Si_4O_{12})_4O_4(OH)_4{\cdot}10H_2O$ which has a deficit of two negative charges. Other possibilities for charge balance are, e.g., replacement of Ba by K and two-valent octahedral cations replacing Ti. Nevertheless, these insufficiencies of an idealized model should not disturb us because the analyzed bulk composition also indicates incomplete occupation of the C (Ba) and the D (Mn) site. Furthermore, the superstructure is very diffuse indicating substantial disorder. This model is also in qualitative agreement with a hypothetical superstructure predicted by Golovastikov (1973). Other closely related structures are those of the organovaite subgroup (Organova et al. 2003; Krivovichev et al., unpublished), which were refined in space group *C*2/*m*. The *I*2/*m* setting used for consistency in this study can be transformed into a *C*2/*m* standard setting (used by Organova et al. 2003) by applying the matrix $[\bar{1}0\bar{1}; 010; 100]$.

Model of a *C*2/*m* structure with *c* = 15.5 Å

Evidence for this model are the extremely sharp but also very weak reflections observed in the diffraction pattern of sample A within the diffuse $l = 2n + 1$ layers. The observed pattern allows us to predict the Ba, Mn distribution at the extraframework sites but the observed intensities are too weak to derive an ordered model for the H_2O (W1, W2) and Na positions. Thus there is a choice between two ordered H_2O and Na arrangements. There is either NaA bonded to W1 and W2 (both H_2O sites fully occupied) or Na' A bonded to W1' and W2'. The assumed composition of the *C*2/*m* structure model $Na_4K_4Ba_2MnTi_8[Si_4O_{12}]_4(O,OH)_8 \cdot 10H_2O$ is identical to the *I*2/*m* structure.

Significance and limitations of the models

If in a "crystal," which does not represent a chemical end-member, diffuse superstructure reflections indicate extensive structural faults it remains unclear whether these defects are purely structural (e.g., polytypism) or also of chemical origin (e.g., submicroscopic domains of slightly different composition). For these reasons the superstructures were modeled for simplified compositions of labuntsovite-lemmleinite solid-solution members. Another major simplification is that diffuse scattering was treated exactly the same way as Bragg diffraction and no information was obtained about the type and spatial correlation of domains and defects leading to the strongly intensity-modulated diffuse features. Nevertheless, the Bragg model derived from crystal-chemical principles is a useful starting point for the understanding of complex disorder phenomena in a complicated chemical system.

We emphasize that the diffuse reciprocal layers are mainly due to partial extraframework order and the average intensity in these layers is governed by the scattering power of the partially ordered heavy elements: Ba at the C site and Fe, Mn, Mg at the D site. This partial extraframework order is primarily determined by the ordered OH, O distribution at O2, required for charge balance, within the chains of TiO_6 octahedra. Recently, Döbelin and Armbruster (2003) reported a similar case in Cd-exchanged heulandite where the Na-exchanged precursor phase exhibited only sharp Bragg reflections whereas the Cd-exchanged crystal displayed additional diffuse superstructure reflections indicating partial long-range order of Cd within the structural cavities.

SYMMETRY AND NOMENCLATURE OF LABUNTSOVITE-GROUP MINERALS

Organova's classification of the diffraction patterns of labuntsovite-group minerals into three groups (see above) was published in 1980. However, most subsequent structural studies of labuntsovite-group minerals (Rastsvetaeva et al. 1994, 1996, 1998, 2001, etc.; Raade et al. 2002) were performed with the monoclinic *C*-centered cell with $c \sim 7.75$ Å. As all these studies were performed using four-circle automated diffractometers, the diffuse diffraction features were either overlooked or ignored. However, even for the Bragg reflections the reported strategy of data collection is of interest and deserves a brief description. Rastsvetaeva et al. (1994) noted that in some labuntsovite-group minerals there are reflections that double the *c* parameter. Existence of these reflections was assigned to effects of twinning and the intensity data were collected in the pseudo-orthorhombic *F* cell with $a_{or} \sim 14.5$, $b_{or} \sim 14.0$, $c_{or} \sim 27$–28 Å. The data were then re-indexed in the "small" *C* cell by applying the [100/010/-$^1/_4$0$^1/_4$] transformation and twinning was introduced into the refinement using the [100/010/$\bar{1}0\bar{1}$] matrix. In the case of a $F \rightarrow C$ transformation using the matrix [100/010/$^1/_4$0$^1/_4$], the transformation of reflection indices can be described as follows: $h_C = h_F$, $k_C = k_F$, $l_C = {}^1/_4(l_F - h_F)$, where h_C, k_C, l_C and h_F, k_F, l_F are indices in the *C* and *F* cells, respectively. As reflection indices should be integers, it is obvious that all reflections with $l_F - h_F \neq 4n$ are rejected during the $F \rightarrow C$ transformation. This seriously questions validity of the transformation process proposed by Rastsvetaeva et al. (1994, 1996) and, consequently, the results of the structure refinement in the "small" *C*-centered cell.

The assumed twinning in labuntsovite-group minerals (monoclinic crystals emulating orthorhombic symmetry due to metric merohedry) is actually rather common in minerals and inorganic compounds. It was found, e.g., in cafetite (Krivovichev et al. 2003), jonesite (Krivovichev and Armbruster 2004), and some synthetic members of the zippeite group (Burns et al. 2003). However, in no case did it result in a doubling of the *c* parameter.

Recently, four new minerals of the labuntsovite group were structurally characterized using intensity data collected with a CCD (charge-coupled device) area detector: organovaite-Mn (Chukanov et al. 2001a), organovaite-Zn (Pekov et al. 2002), parakuzmenkoite-Fe (Chukanov et al. 2001b), and paratsepinite-Ba (Chukanov et al. 2003). The crystal structures of these four minerals were refined in a cell with a doubled *c* dimension and space group *C*2/*m* (equivalent to the *I*2/*m* space group by applying the transformation matrix [$\bar{1}0\bar{1}$/010/100]). Obviously, the doubled *c* parameter is in agreement with the results reported by Rastsvetaeva et al. (1994, 1996) for other labuntsovite-group minerals. However, application of a CCD area detector allowed collection of a full set of Bragg diffraction data for the four new minerals (Chukanov et al. 2001a; Pekov et al. 2002; Chukanov et al. 2001b; Chukanov et al. 2003). Attempts to transform data sets of space group *C*2/*m* (= *I*2/*m*) with $c \sim 15.5$ Å, collected with a CCD detector, to the smaller *C* cell with $c \sim 7.75$ Å resulted in rejection of several hundreds of observed reflections and thus was found to be inappropriate (Organova et al. 2003). In addition, the refinement in the smaller cell using partial data resulted in higher *R*-values than in the doubled cell, yielding disordered extraframework positions and unreliable atomic displacement parameters (Organova et al. 2003). Furthermore, a structure model for a cell with $c \sim 15.5$ Å shows an ordered arrangement of the extraframework cations.

We recommend that all samples for which a doubled cell has been observed but ignored (e.g., samples studied by Rastsvetaeva et al. 1994, 1996, 2001, etc.) should be re-studied using an area detector that allows collection of all Bragg diffraction data and even diffuse scattering data. This could lead to the refined nomenclature scheme proposed by Chukanov et al. (2002) for the labuntsovite group. It seems likely that at least transitional labuntsovite-lemmleinite members of the group may exist in both ordered and disordered modifications with a range of structures with an intermediate degree of order.

ACKNOWLEDGMENTS

S.V.K. thanks the Alexander von Humboldt Foundation for partial financial support and the Swiss National Science Foundation for support during stay at Bern (Grant 20-65084.01 to T.A., Crystal Chemistry of Minerals).

REFERENCES CITED

Armbruster, T. (1986) Crystal structure refinement and thermal expansion of a Li,Na,Be-cordierite between 100 and 550 K. Zeitschrift für Kristallographie, 174, 205–217.

Bruker AXS (1998) SHELXTL Version 5.1.

Burns, P.C., Deely, K.M., and Hayden, L.A. (2003) The crystal chemistry of the zippeite group. Canadian Mineralogist, 41, 687–706.

Chukanov, N.V., Pekov, I.V., Rastsvetaeva, R.K., and Nekrasov, A.N. (1999) Labuntsovite: solid solutions and features of the crystal structure. Canadian Mineralogist, 37, 901–910.

Chukanov, N.V., Pekov, I.V., Zadov, A.E., Krivovichev, S.V., Burns, P.C., and Schneider, J. (2001a) Organovaite-Mn, $K_2Mn(Nb,Ti)_4(Si_4O_{12})_2(O,OH)_4 \cdot 6H_2O$, a new labuntsovite group mineral from Lovozero massif, Kola peninsula. Zapiski Vsesoyuznogo Mineralogicheskogo Obschestva, 130(2), 46–53.

Chukanov, N.V., Pekov, I.V., Semenov, E.I., Zadov, A.E., Krivovichev, S.V., and Burns, P.C. (2001b) Parakuzmenkoite-Fe, $(K,Ba)_2Fe(Ti,Nb)_4(Si_4O_{12})_2(O,OH)_4 \cdot 7H_2O$, a new labuntsovite group mineral. Zapiski Vsesoyuznogo Mineralogicheskogo Obschestva, 130(2), 63–67.

Chukanov, N.V., Pekov, I.V., and Khomyakov, P. (2002) Recommended nomenclature for labuntsovite-group minerals. European Journal of Mineralogy, 14, 165–173.

Chukanov, N.V., Pekov, I.V., Zadov, A.E., Rozenberg, K.A., Rastsvetaeva, R.K., Krivovichev, S.V., and Levitskaya, L.A. (2003) New minerals tsepinite-K $(K,Ba,Na)_2(Ti,Nb)_2(Si_4O_{12})(OH,O)_2 \cdot 3H_2O$ and paratsepinite-Ba $(Ba,Na,K)_{2-x}(Ti,Nb)_2(Si_4O_{12})(OH,O)_2 \cdot 4H_2O$ and their relationship with other labuntsovite group members. Zapiski Vserossiiskogo Mineralogicheskogo Obshchestva, 132(1), 38–51.

Döbelin, N. and Armbruster, T. (2003) Stepwise dehydration and change of framework topology in Cd-exchanged heulandite. Microporous and Mesoporous Materials, 61, 85–103.

Enraf-Nonius (1982) SDP Structure determination package.

Estermann, M.A. and Steurer, W. (1998) Diffuse scattering data acquisition techniques. Phase Transitions, 67, 165–195.

Golovastikov, N.I. (1973) Crystal structure of the alkali titanosilicate labuntsovite. Kristallografiya, 18, 950–955.

Herbstein, F.H. (2000) How precise are measurements of unit-cell dimensions from single-crystals. Acta Crystallographica, B56, 547–557.

Krivovichev, S.V. and Armbruster, T. (2004) The crystal structure of jonesite, $Ba_2(K,Na)[Ti_2(Si_5Al)O_{18}(H_2O)](H_2O)_n$: a first example of titanosilicate with porous double layers. American Mineralogist, 89, 314–318.

Krivovichev, S.V., Yakovenchuk, V.N., Burns, P.C., Pakhomovsky, Ya.A., and Menshikov, Yu.P. (2003) Cafetite, $Ca[Ti_2O_5](H_2O)$: crystal structure and revision of chemical formula. American Mineralogist, 88, 424–429.

Kunz, M. and Brown, I.D. (1995) Out-of-center distortions around octahedrally coordinated d_0 transition metals. Journal of Solid State Chemisty, 115, 395–406.

Milton, C., Mrose, M.E., Fahey, J.J., and Chao, E.C.T. (1958) Labuntsovite from the trona mine, Seawater County, Wyoming. Bulletin of the Geological Society of America, 64, 1614–1615.

Organova, N.I., Shlyukova, Z.V., Zabavnikova, N.I., Platonov, A.N., and Rudnitskaya, E.S. (1976) On crystal chemistry of labuntsovite and nenadkevichite. Ivestiya Akademii Nauk SSSR, Seriya Geologicheskaya, 2, 98–116.

Organova, N.I., Shlyukova, Z.V., and Tsepin, A.I. (1980) Crystal chemistry of disorder in labuntsovites. In T.N. Shadlun, Ed., Uporyadochenie i Raspad Tverdykh Rastvorov v Mineralah. Nauka: Moscow, pp. 39–57.

Organova, N.I., Arkhipenko, D.K., Dikov, Yu.P., Karpinsky, O.G., and Shlyukova, Z.V. (1981) Structural features of a new K-bearing variety of labuntsovite, and its place in labuntsovite-nenadkevichite family. Mineralogicheskiy Zhurnal, 2, 49–63.

Organova, N.I., Krivovichev, S.V., Shlyukova, Z.V., Zadov, A.E., Rozhdestvenskaya, I.V., and Ivanova, T.I. (2003) Structure of "parazepinite-Na" and its place between the minerals of the labuntsovite group. Crystallography Reports, accepted.

Pekov, I.V., Chukanov, N.V., Zadov, A.E., Krivovichev, S.V., Azarova, Yu.V., Burns, P.C., and Schneider, J. (2002) Organovaite-Zn, $K_2Zn(Nb,Ti)_4(Si_4O_{12})_2(O,OH)_4 \cdot 6H_2O$, a new mineral of the labuntsovite group. Zapiski Vserossiiskogo Mineralogicheskogo Obshchestva, 131(1), 29–34.

Raade, G., Ferraris, G., Gula, A., and Ivaldi, G. (2002) Gjerdingenite-Fe from Norway, a new mineral species in the labuntsovite group: description, crystal structure and twinning. Canadian Mineralogist, 40, 1629–1639.

Rastsvetaeva, R.K., Tamazyan, R.A., Pushcharovsky, D.Yu., and Nadezhina, T.N. (1994) Crystal structure and microtwinning of K-rich nenadkevichite. European Journal of Mineralogy, 6, 503–509.

Rastsvetaeva, R.K., Arakcheeva, A.V., and Khomyakov, A.P. (1996) Crystal structure and microtwinning of a new monoclinic analogue of nenadkevichite. Doklady Rossiyskoi Akademii Nauk, 351, 207–211.

Rastsvetaeva, R.K., Chukanov, N.V., and Pekov, I.V. (1997) Crystal structure of new mineral analogue of labuntsovite with high ordering of potassium and barium. Doklady Rossiyskoi Akademii Nauk, 357, 64–67.

Rastsvetaeva, R.K., Chukanov, N.V., Pekov, I.V., Shlyukova, Z.V., and Khomyakov, A.P. (1998) Crystal structures of two potassium-rich labuntsovites and crystal chemistry of labuntsovite-nenadkevichite family minerals. Crystallography Reports, 43, 820–827.

Rastsvetaeva, R.K., Pekov, I.V., and Nekrasov, Yu.V. (2001) Crystal structure and microtwinning of Ca-rich analogue of labuntsovite. Kristallografiya, 46, 415–417.

Semenov, E.I. and Burova, T.A. (1955) On a new mineral, labuntsovite, and so-called titanoelpidite. Doklady Akademii Nauk SSSR, 101, 1113–1116.

Yakovenchuk, V.N., Ivanyuk, G.Yu., Pakhomovsky, Ya.A., and Men'shikov, Yu.P. (1999) Minerals of the Khibina Massif. Moscow, Zemlya.

MANUSCRIPT RECEIVED AUGUST 29, 2003
MANUSCRIPT ACCEPTED JANUARY 17, 2004
MANUSCRIPT HANDLED BY ALESSANDRO GUALTIERI